Schweizerischer Erdbebendienst
Service Sismologique Suisse
Servizio Sismico Svizzero
Swiss Seismological Service

ETH zürich

Basel - Vogelsang (SBAV)

SITE CHARACTERIZATION REPORT

Clotaire MICHEL, Stefano MARANO, Carlo CAUZZI

Valerio POGGI, Jan BURJANEK, Manuel HOBIGER, Donat FÄH

Sonneggstrasse 5 CH-8092 Zürich Switzerland; E-mail: clotaire.michel@sed.ethz.ch

Last modified : July 15, 2015

Abstract

Ambient vibration array measurements were performed to characterize the site Basel Vogelsang, in the Kleinbasel district. The site, where the new station SBAV of the Swiss Strong Motion Network was installed, is located on the alluvia of the Rhine in the city of Basel. The new station was installed in the frame of the Basel Erdbebenvorsorge project. In order to characterize the velocity profile under the station, array measurements with $240\,\mathrm{m}$ aperture were performed. The measurements were successful and allowed deriving velocity models for this site. Inversion with Love and Rayleigh dispersion curves lead to different velocity profiles, with larger velocity values from 6 to $200\,\mathrm{m}$ depth using Love curve. The Quaternary and Tertiary sediments are stiff from $500\,\mathrm{m/s}$ near the surface up to $1400\,\mathrm{m/s}$ at the base of the Tertiary. The interface with the Mesozoic basement takes place between 550 and $650\,\mathrm{m}$ depth. It is producing the fundamental peak in the ellipticity at $0.55\,\mathrm{Hz}$. $V_{s,30}$ is $523\,\mathrm{m/s}$, which would correspond to ground type B in the Eurocode 8 [CEN, 2004] and SIA261 [SIA, 2014]. The theoretical 1D SH transfer function computed from the inverted profiles shows amplifications up to a factor 3 at some resonance frequencies and matches the observed amplification at the station during earthquakes.

Contents

1 Introduction **4**

2 Geology **5**

3 Experiment description **5**

3.1 Ambient Vibrations 5

3.2 Equipment 5

3.3 Geometry of the arrays 6

3.4 Positioning of the stations 6

4 Data quality **7**

4.1 Usable data 7

4.2 Data processing 7

5 H/V processing **8**

5.1 Processing method and parameters 8

5.2 Results 8

5.3 Polarization analysis 9

6 Array processing **11**

6.1 Processing methods and parameters 11

6.2 Obtained dispersion curves 11

7 Inversion and interpretation **15**

7.1 Inversion 15

7.2 Travel time average velocities and ground type 20

7.3 SH transfer function and quarter-wavelength velocity 20

8 Conclusions **23**

References **25**

1 Introduction

The station SBAV (Basel - Vogelsang) is part of the dense array of the Swiss Strong Motion Network (SSMNet) in Basel. SBAV has been installed in the framework of the Basel Erdbebenvorsorge project in 2013 as a new station. This project also includes the site characterization. Passive array measurements have been selected as a standard tool to investigate these sites. An array measurement campaign was carried out on 4th July 2013 in the area of the school Vogelsang (Fig. 1), with a centre close to SBAV, in order to characterize the velocity profile under this station. This station is located on the flat alluvial plain of the Rhine. This report presents the measurement setup, the results of the H/V analysis and of the array processing of the surface waves (dispersion curves). Then, an inversion of these results into velocity profiles is performed. Standard parameters are derived to evaluate the amplification at this site.

Canton	City	Location	Station code	Site type	Slope
Basel Stadt	Basel	Vogelsang	SBAV	Alluvial plain	Flat

Table 1: Main characteristics of the study-site.

Figure 1: Picture of the site.

2 Geology

The station is located within the deep Rhine graben where resonance from Tertiary and Quaternary sediments is expected. Moreover, it is located in the deepest part of the St Jakob-Tüllingen syncline with deeper Tertiary deposits. The geological map indicates that the site is located on the Quaternary alluvia of the Rhine. A borehole nearby is showing that the quaternary sediments are approximately $18\,\mathrm{m}$ thick and lay on the Cyrenenmergel layer (molassic marls and sands of late Rupelian age, Tertiary) or the Septarienton formation (formerly known as Meletta layer or Blauer Letten, calcareous mudstone of Rupelian age) depending on the sources. They are both part of the "series grises", down to the Sannoisian marl at approximately $360\,\mathrm{m}$ depth based on interpolation. This marl was formerly assumed as the geophysical bedrock. Following the interpretation of the Otterbach-2 VSP measurement, the geophysical basement is supposed to be the Mesozoic basement (limestone). It is expected between 500 and $650\,\mathrm{m}$ depth from cross-sections of the syncline.

3 Experiment description

3.1 Ambient Vibrations

The ground surface is permanently subjected to ambient vibrations due to:

- natural sources (ocean and large-scale atmospheric phenomena) below $1\,\mathrm{Hz}$,
- local meteorological conditions (wind and rain) at frequencies around $1\,\mathrm{Hz}$,
- human activities (industrial machines, traffic…) at frequencies above $1\,\mathrm{Hz}$ [Bonnefoy-Claudet et al., 2006].

The objective of the measurements is to record these ambient vibrations and to use their propagation properties to infer the underground structure. First, the polarization of the recorded waves (H/V ratio) is used to derive the resonance frequencies of the soil column. Second, the arrival time delays at many different stations are used to derive the velocity of surface waves at different frequencies (dispersion). The information (H/V, dispersion curves) is then used to derive the properties of the soil column using an inversion process.

3.2 Equipment

For these measurements 11 Quanterra Q330 dataloggers named NR01 to NR12 (except NR08) and 14 Lennartz 3C 5 s seismometers were available (see Tab. 2). Each datalogger can record on 2 ports A (channels EH1, EH2, EH3 for Z, N, E directions) and B (channels EH4, EH5, EH6 for Z, N, E directions). Time synchronization was ensured by GPS. The sensors were placed on a metal tripod, in a $20\,\mathrm{cm}$ deep hole, when possible, for better coupling with the ground.

Digitizer	Model	Number	Resolution
	Quanterra Q330	11	24 bits
Sensor type	**Model**	**Number**	**Cut-off frequency**
Velocimeter	Lennartz 3C	14	0.2 Hz

Table 2: Equipment used.

3.3 Geometry of the arrays

Two array configurations were used, for a total of 4 rings of 10, 30, 60 and 120 m radius around a central station. The first configuration includes the 3 inner rings with 14 sensors; the second configuration includes the 2 outer rings (plus 1 sensor of the first ring) with 12 sensors. The minimum inter-station distance and the aperture are therefore 10 and 120 m and 10 and 240 m, respectively. The experimental setup is displayed in Fig. 2. The final usable datasets are detailed in section 4.2.

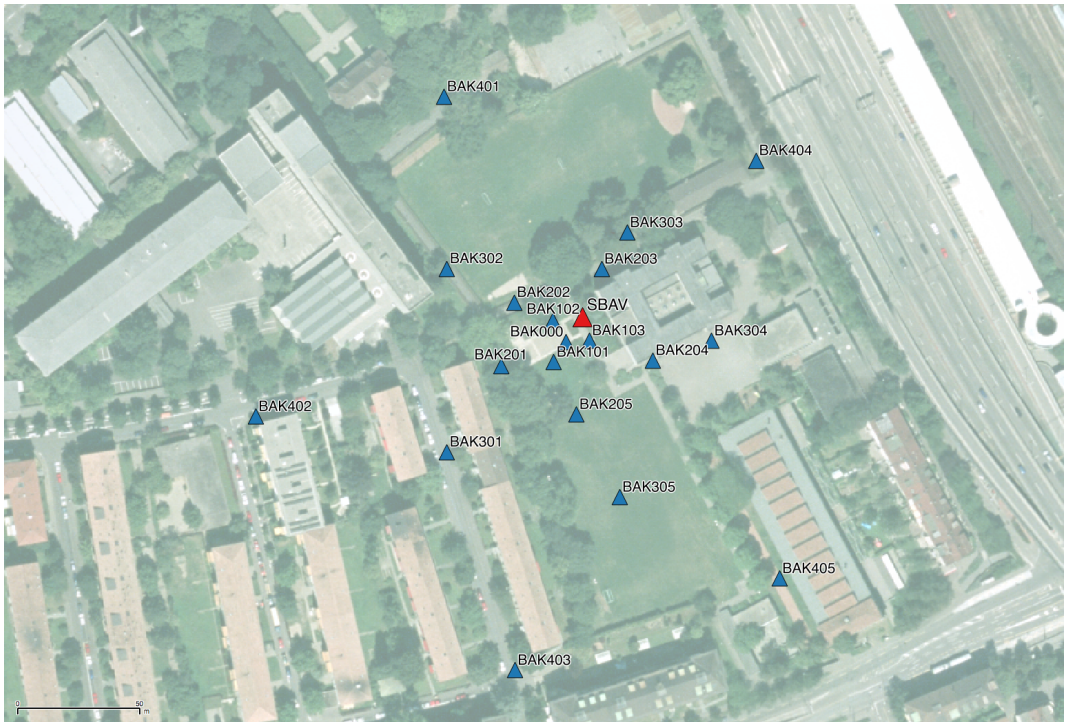

Figure 2: Geometry of the arrays.

3.4 Positioning of the stations

The sensor coordinates were measured using a differential GPS device (Leica Viva GS10), including only a rover station and using the Real Time Kinematic technique provided by Swisstopo. It allows an absolute positioning with an accuracy better than 3 cm on the Swissgrid. However, this accuracy was not reached at some points due to trees (BAK201 with 18 cm, BAK203 with 24 cm, BAK301 with 41 cm, BAK303 with 27 cm, BAK401 with 18 cm and

BAK403 with $19\,\mathrm{cm}$). It can be noticed that the second configuration has been measured using the LV95 system instead of the LV03 and had therefore to be corrected.

4 Data quality

4.1 Usable data

The largest time windows were extracted, for which all the sensors of the array were correctly placed and the GPS synchronization was ensured. Recordings are very consistent up to $10\,\mathrm{Hz}$. Local noise sources are located between 10 and $20\,\mathrm{Hz}$. Point BAK404, close to the highway, is noticeably more noisy. During the last 5-10 minutes of dataset 1, the lawn was mown on the football field. During dataset 2, several groups played football within the array. Spurious peaks at 1.13. 4.55 and $8.3\,\mathrm{Hz}$ are noticed as for many other sites in Basel.

Orientations of the sensors were checked by maximizing the correlation with the central station at low frequencies [Poggi et al., 2012b]. Deviations lower than $9\,^\circ$ were found for all points but BAK405 ($14\,^\circ$). Original and rotated datasets are available for the 3C array analysis.

The characteristics of the datasets are detailed in Tab. 3.

4.2 Data processing

The data were first converted to SAC format including in the header the coordinates of the point (CH1903 system), the recording component and a name related to the position. The name is made of 3 letters characterizing the location (BAK here), 1 digit for the ring and 2 more digits for the number in the ring. Recordings were not corrected for the full instrumental response but only for a conversion factor.

Dataset	Starting Date	Time	Length	F_s	Min. inter-distance	Aperture	# of points
1	2013/07/04	09:49	131 min	200 Hz	10 m	120 m	14
2	2013/07/04	12:37	126 min	200 Hz	10 m	240 m	12

Table 3: Usable datasets.

5 H/V processing

5.1 Processing method and parameters

In order to process the H/V spectral ratios, several codes and methods were used. The classical H/V method was applied using the Geopsy `http://www.geopsy.org` software. In this method, the ratio of the smoothed Fourier Transform of selected time windows are averaged. Tukey windows (cosine taper of 5% width) of $50\,\mathrm{s}$ long overlapping by 50% were selected. Konno and Ohmachi [1998] smoothing procedure was used with a b value of 60. The classical method computed using the method of Fäh et al. [2001] was also performed.

Moreover, the time-frequency analysis method [Fäh et al., 2009] was used to estimate the ellipticity function more accurately using the Matlab code of V. Poggi. In this method, the time-frequency analysis using the Wavelet transform is computed for each component. For each frequency, the maxima over time (10 per minute with at least $0.1\,\mathrm{s}$ between each) in the TFA are determined. The Horizontal to Vertical ratio of amplitudes for each maximum is then computed and statistical properties for each frequency are derived. A Cosine wavelet with parameter 9 is used. The mean of the distribution for each frequency is stored. For the sake of comparison, the time-frequency analysis of Fäh et al. [2001], based on the spectrogram, was also used, as well as the wavelet-based TFA coded in Geopsy.

The ellipticity extraction using the Capon analysis [Poggi and Fäh, 2010] (see section on array analysis) was also performed as well using the wavefield decomposition method [Maranò et al., 2012].

Method	Freq. band	Win. length	Anti-trig.	Overlap	Smoothing
Standard H/V Geopsy	$0.2 - 20\,\mathrm{Hz}$	$50\,\mathrm{s}$	No	50%	K&O 60
Standard H/V D. Fäh	$0.2 - 20\,\mathrm{Hz}$	$30\,\mathrm{s}$	No	75%	-
H/V TFA Geopsy	$0.2 - 20\,\mathrm{Hz}$	Morlet m=8 fi=1	No	-	-
H/V TFA D. Fäh	$0.2 - 20\,\mathrm{Hz}$	Specgram	No	-	-
H/V TFA V. Poggi	$0.2 - 20\,\mathrm{Hz}$	Cosine wpar=9	No	-	No

Table 4: Methods and parameters used for the H/V processing.

5.2 Results

All points show the same shape in their H/V below $5\,\mathrm{Hz}$ with a complex right flank (Fig. 3). The fundamental peak, picked in the centre of the whole peak, not at the highest point, is found at $0.55\,\mathrm{Hz}$. It corresponds to the resonance of the deep Rhine graben.

Moreover, all the methods to compute H/V ratios are compared at the array centre on Fig. 4, in which the classical methods were divided by $\sqrt{2}$ to correct from the Love wave contribution [Fäh et al., 2001]. The classical and TFA methods match well at high frequencies but large variations are observed at low frequencies. The 3C FK analysis (Capon method) does not have resolution down to the peak but matches perfectly with the H/V analysis at high frequency. The wave field decomposition method is also presented here with similar results, except below the

array limit for the small configuration. It is less smooth than the FK results, following more closely the H/V ratios. The sign of the ellipticity shows that the polarization of Rayleigh waves is retrograde on the whole spectra, no singularity is found at the trough.

The fundamental peak at the SBAV station is therefore at $0.55\,\mathrm{Hz}$, with a peak amplitude around 3 for the TFA methods.

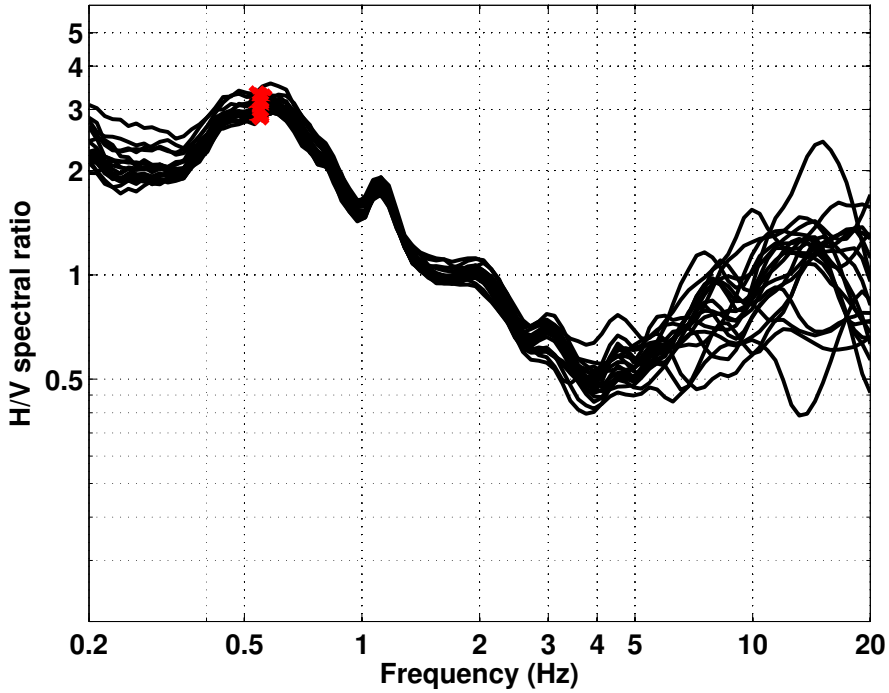

Figure 3: H/V spectral ratios (time-frequency analysis code V. Poggi) of all array points.

5.3 Polarization analysis

Considering the shape of the Rhine basin, a 2D resonance could occur. Therefore, polarization analysis on the array data was performed using the method of Burjánek et al. [2010]. The polarization of the spurious peak at $1.13\,\mathrm{Hz}$ observed everywhere in Basel is clearly visible. No point (Fig. 5) shows a noticeable polarization at $0.5\,\mathrm{Hz}$ perpendicular to the Rhine graben. 2D resonance is therefore unlikely at this location.

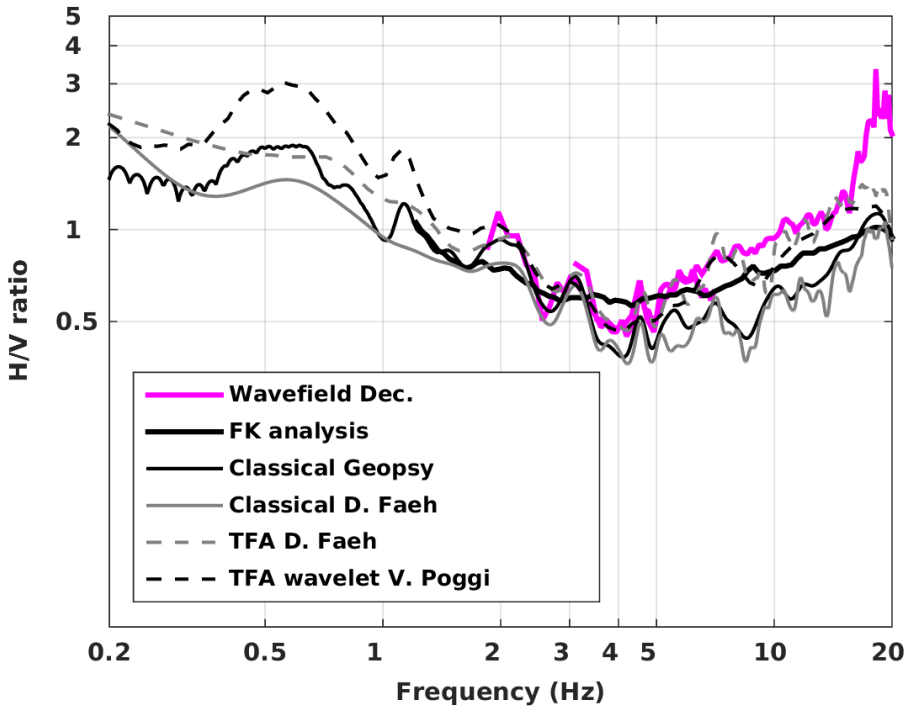

Figure 4: H/V spectral ratios for point BAK000 using the different codes. Classical methods were divided by $\sqrt{2}$.

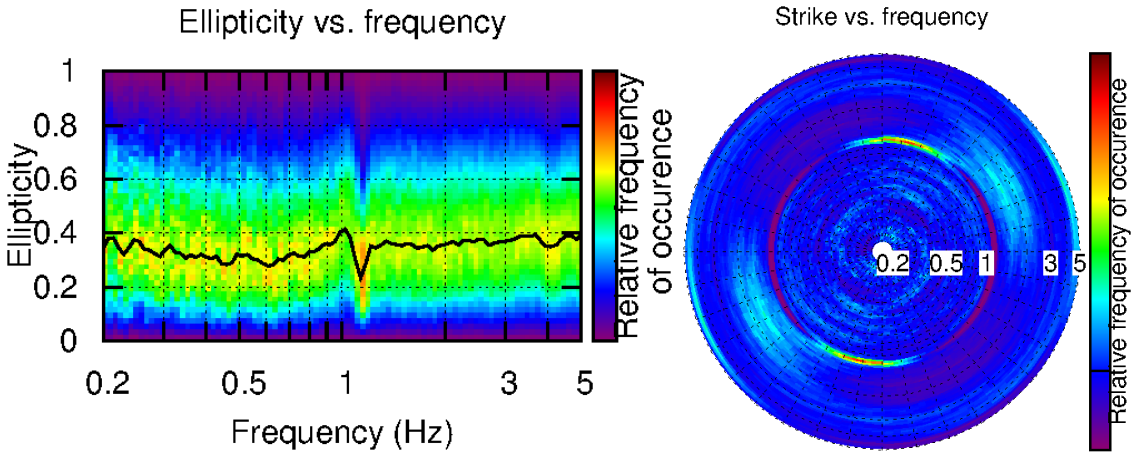

Figure 5: Polarization analysis at point BAK000. Left: Ellipticity (A trough in the ellipticity corresponds to polarized motion). Right: Strike of the polarization.

6 Array processing

6.1 Processing methods and parameters

The vertical components of the arrays were processed using the FK and the High-resolution FK analysis [Capon, 1969] using the Geopsy `http://www.geopsy.org` software. Better results were obtained using large time windows (300T). The results of computations of both datasets were merged to estimate the dispersion curves.

Moreover, a 3C array analysis [Fäh et al., 2008] was also performed using the array_tool_3C software [Poggi and Fäh, 2010]. It allows us to derive Rayleigh and Love modes including the Rayleigh ellipticity. The results of computations of both datasets were merged to estimate the dispersion curves.

The array was also processed following the method proposed in Maranò et al. [2012]. Results are obtained modeling propagating plane waves at each time window and frequency. The recording is split in windows of 20 seconds. Parameter estimation is done via maximum likelihood. Model selection (choice of wave type and number of waves) is performed using the Bayesian information criterion.

Method	Set	Freq. band	Win. length	Anti-trig.	Overlap	Grid step	Grid size	# max.
HRFK 1C	1	$1-25\,\mathrm{Hz}$	$300T$	No	50%	0.001	0.6	5
HRFK 1C	2	$1-25\,\mathrm{Hz}$	$300T$	No	50%	0.001	0.6	5
HRFK 3C	1	$1-25\,\mathrm{Hz}$	Wav. 10 Tap. 0.2	No	50%	300 m/s	2000 m/s	5
HRFK 3C	2	$1-25\,\mathrm{Hz}$	Wav. 10 Tap. 0.2	No	50%	300 m/s	2000 m/s	5
Wavef. dec.	1&2	$0-20\,\mathrm{Hz}$	20s					

Table 5: Methods and parameters used for the array processing.

6.2 Obtained dispersion curves

In the 1C FK analysis, the fundamental Rayleigh mode could be picked between 1.2 and $20\,\mathrm{Hz}$ (Fig. 6), including its standard deviation. The velocities range from $1200\,\mathrm{m/s}$ at $1.2\,\mathrm{Hz}$ down to $430\,\mathrm{m/s}$ at $20\,\mathrm{Hz}$. A higher mode can also be clearly picked but its order is unknown.

Using the 3C analysis, fundamental Rayleigh mode can be picked as previously (Fig. 6). On the radial component the same mode is seen and a higher mode can be picked. On the transverse component, the fundamental Love mode is picked.

All picked curves are presented together on Fig. 7. The fundamental and higher Rayleigh modes are identical for 1C and 3C analysis. Moreover, the finally selected curves (Love and Rayleigh) are compared to the picked curves from the wave field decomposition method (two datasets Fig. 8). It can be noticed that the Rayleigh fundamental mode from wavefield decomposition is biased outside of the array limits. This method also does not see the bump in the fundamental Rayleigh mode at $2.5\,\mathrm{Hz}$ that may just be an artifact from the FK analysis. The

histograms to retrieve Love dispersion curves are more scattered in both methods, resulting in a significant difference in the picking (more automatic in the wave field decomposition and more manual in the FK) of about 7%.

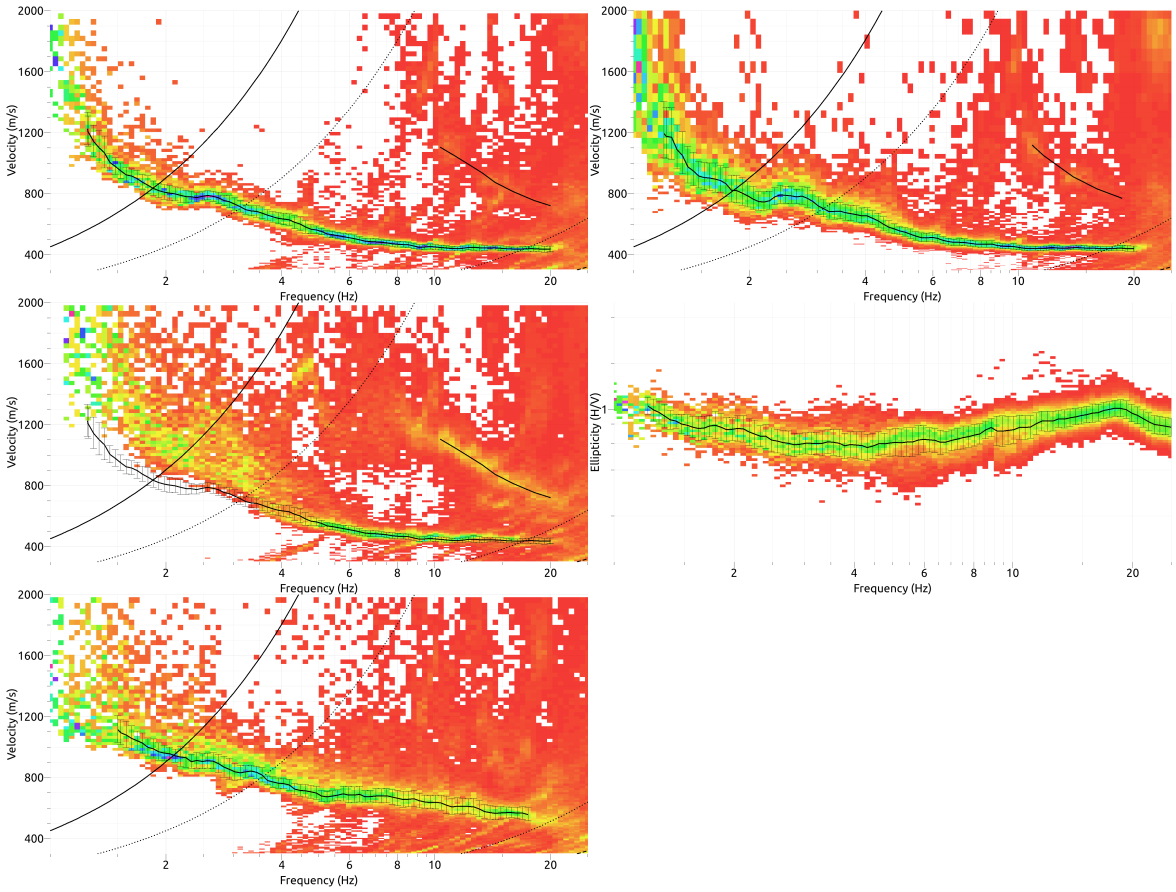

Figure 6: Dispersion curves and ellipticity obtained from the 3C and 1C array analyses (from top to bottom: vertical, radial, transverse components; left: 3C analysis; top right: 1C analysis; centre right: ellipticity).

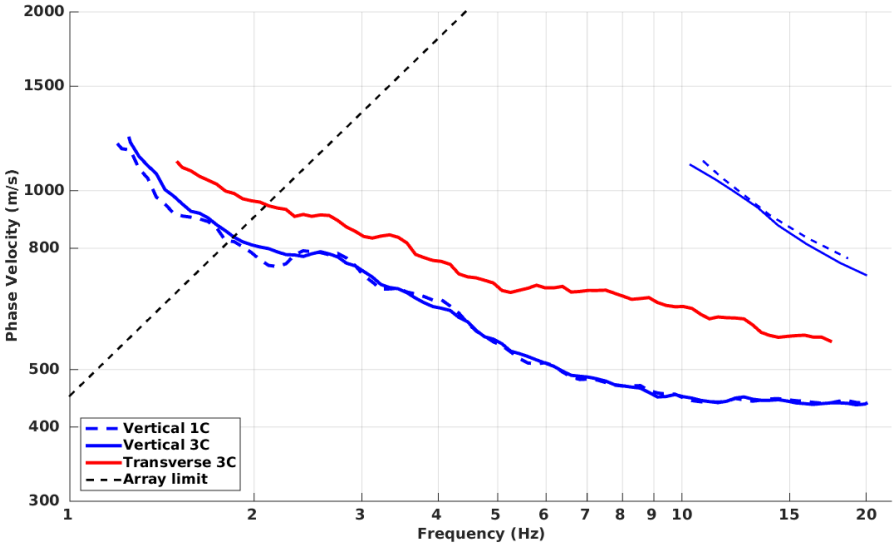

Figure 7: Picked dispersion curves from 1C and 3C FK methods.

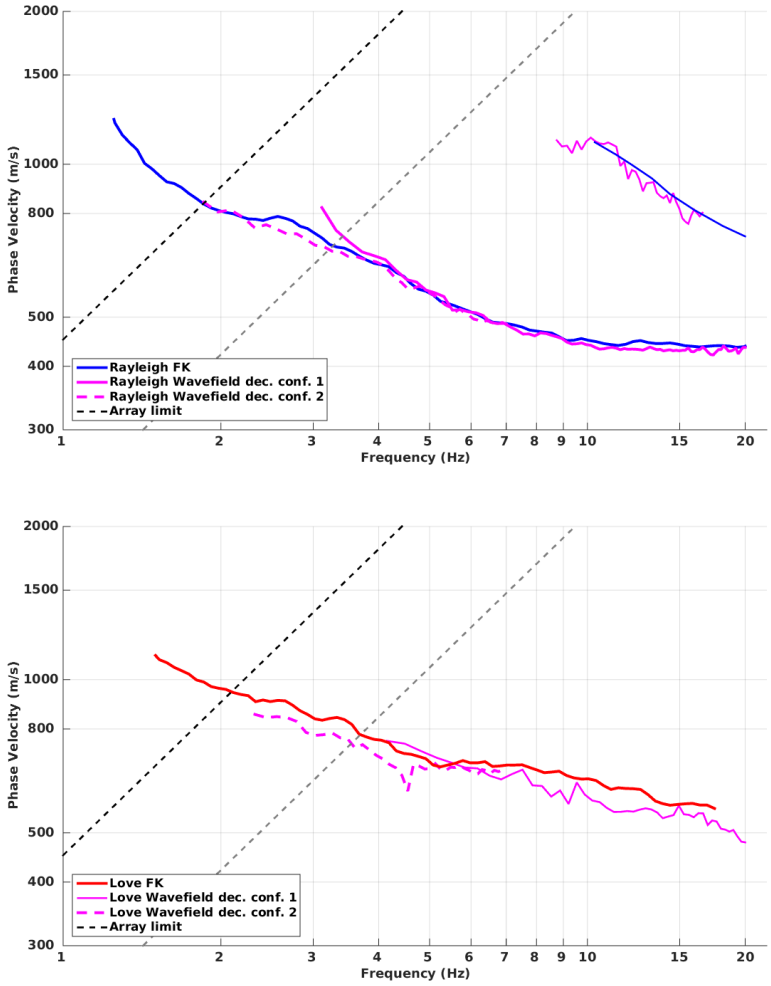

Figure 8: Selected dispersion curves from the FK analyses compared to the obtained curves using the wave field decomposition method. Top: Rayleigh dispersion; Bottom: Love dispersion.

7 Inversion and interpretation

7.1 Inversion

For the inversion, the Rayleigh fundamental dispersion curve, the ellipticity curve (TFA Poggi) and the fundamental frequency at $0.55\,\mathrm{Hz}$ were used as simultaneous targets without standard deviation. The higher mode of Rayleigh dispersion found in the FK analysis is most probably the second higher and was not used because of its uncertainty. After many tests, the fundamental Love dispersion curve was discarded for this computation. As in many other locations in Basel, this curve is not compatible with the other targets (too high velocities). A possible explanation could be anisotropy (vertical vs horizontal) in the mudstone of the Septarienton formation. A second inversion was performed using the Love dispersion curve instead of Rayleigh, without using the ellipticity curve.

A weight of 0.5 and 0 was assigned to the ellipticity curve and 0.1 and 0.3 to the ellipticity peak for these two inversions, respectively. All curves were resampled using 50 points between 0.3 and $22\,\mathrm{Hz}$ in log scale.

The inversion was performed using the Improved Neighborhood Algorithm (NA) [Wathelet, 2008] implemented in the Dinver software. In this algorithm, the tuning parameters are the following: Ns_0 is the number of starting models, randomly distributed in the parameter space, Nr is the the number of best cells considered around these Ns_0 models, Ns is the number of new cells generated in the neighborhood of the Nr cells (Ns/Nr per cell) and It_{max} is the number of iteration of this process. The process ends with $Ns_0 + Nr * \frac{Ns}{Nr} * It_{max}$ models. The used parameters are detailed in Tab. 6.

It_{max}	Ns_0	Ns	Nr
500	10000	100	100

Table 6: Tuning parameters of Neighborhood Algorithm.

No velocity inversion is needed to explain the data although it could be expected at some interfaces. The Poisson ratio was inverted in each layer in the range 0.2-0.4, up to 0.47 in the alluvia, within the groundwater table. The density was assumed to be $2000\,\mathrm{kg/m^3}$ in the sediments and $2700\,\mathrm{kg/m^3}$ in the Mesozoic rock. The velocity of the bedrock is assumed to be $2340\,\mathrm{m/s}$ (from the Otterbach 2 VSP measurement). Inversions with free layer depths as well as fixed layer depths were performed. 4 layers are enough to explain most of the targets (dispersion and ellipticity), but more layers are used to smooth the obtained results and better explore the parameter space. For each assumption (Rayleigh or Love dispersion), 5 independent runs of 5 different parametrization schemes (6 and 7 layers over a half space and 13, two times 15 layers with fixed depth with different values) were performed. Examples of retrieved ground profiles for these two strategies are presented in Fig. 9. When comparing to the target curves for the inversion with the Rayleigh curve (Fig. 10), the Rayleigh fundamental mode is well represented. The higher mode is of higher order than 2 and therefore not used in the inversion. As explained above, the fundamental Love mode is not compatible with this velocity profile. The inversion with Love curve (Fig. 11) also leads to a good fit of the dispersion curve and

even the ellipticity though it was not used in the inversion. None of both inversions is better at reproducing the data.

For further elaborations, the best models of these 2 times 25 runs were selected (Fig. 12). The first meter of the profile shows low velocities, the lowest allowed in the inversion (about $200\,\mathrm{m/s}$). Below, the velocity is around $490\,\mathrm{m/s}$ until $6\,\mathrm{m}$ depth. Using the Rayleigh dispersion, the velocity does not increase down to approximately $45\,\mathrm{m}$, whereas using the Love dispersion curve, it rises to $670\,\mathrm{m/s}$. No contrast between Quaternary and Tertiary sediments can be seen. With the Rayleigh dispersion, a sharp contrast is clearly seen at $45\,\mathrm{m}$ depth with velocity jumping up to more than $800\,\mathrm{m/s}$. With Love dispersion, the contrast occurs slightly deeper, at $60\,\mathrm{m}$ depth, with velocities increasing up to $1100\,\mathrm{m/s}$. In previous works, the first $50\,\mathrm{m}$ with low velocities were interpreted as weathered Tertiary rock and can be seen everywhere in Basel with slightly varying depths.

Below, the velocity increase is less constrained. Profiles with Rayleigh and Love curves meet between 150 and $250\,\mathrm{m}$ depth. The velocity reaches $1400\,\mathrm{m/s}$ at $400\,\mathrm{m}$ depth and does not seem to exceed much this value in the Tertiary layers. Finally, the bedrock is found between 550 and $650\,\mathrm{m}$ depth, as expected.

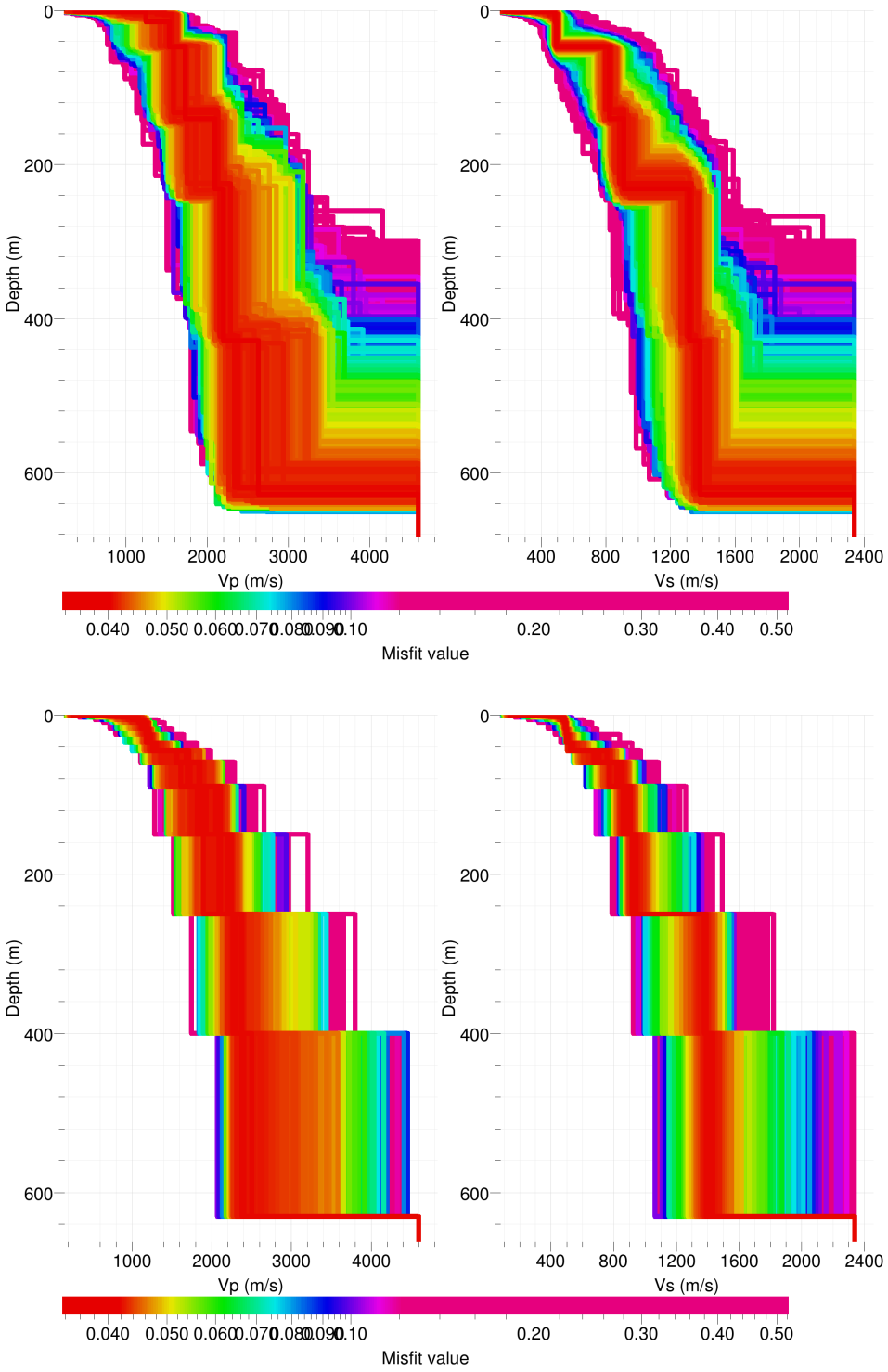

Figure 9: Inverted ground profiles in terms of V_p and V_s; top: free layer depth strategy; bottom: fixed layer depth strategy.

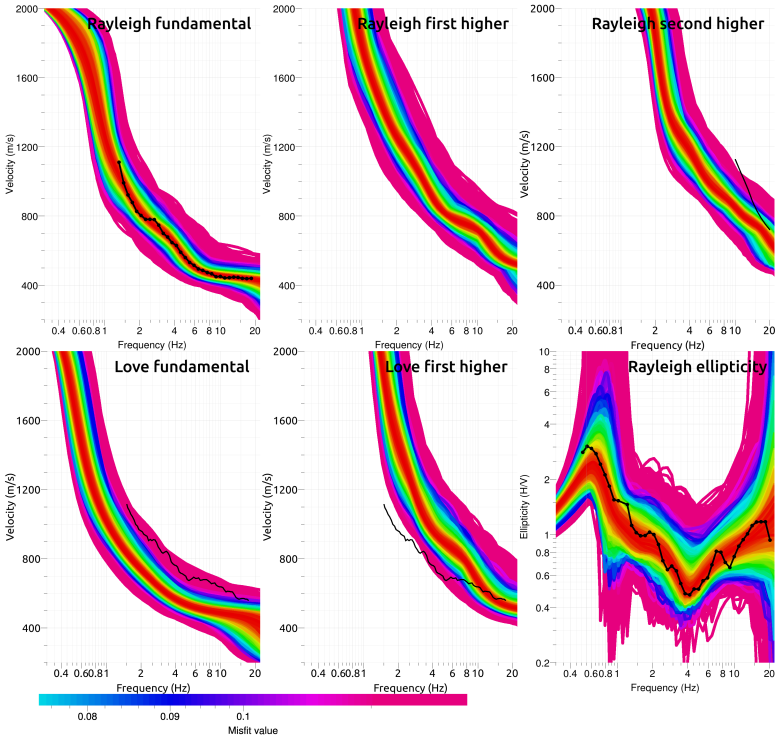

Figure 10: Inversion with Rayleigh curves: comparison between inverted models and measured Rayleigh and Love modes and corresponding ellipticity. Thin black lines were not used in the inversion.

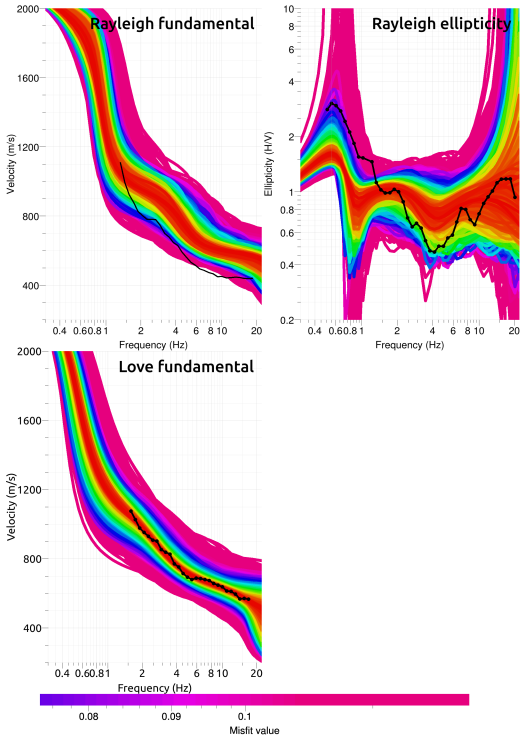

Figure 11: Inversion with Love curves: comparison between inverted models and measured Rayleigh and Love modes and corresponding ellipticity. Thin black lines were not used in the inversion.

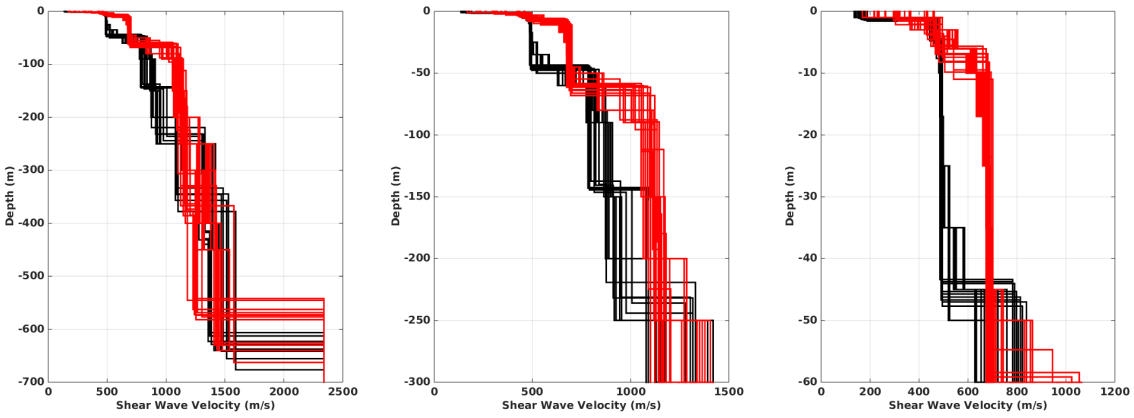

Figure 12: V_s ground profiles for the selected 50 best models. Models from the inversion with Rayleigh (black) and Love (red) curves.

7.2 Travel time average velocities and ground type

The distribution of the travel time average velocities at different depths was computed from the selected models. The uncertainty, computed as the standard deviation of the distribution of travel time average velocities for the considered models, is also provided. $V_{s,30}$ is found to be $523\,\mathrm{m/s}$, which corresponds to class B in the Eurocode 8 [CEN, 2004] and the SIA261 [SIA, 2014]. It should however be noticed that this value corresponds to an average between the inverted profiles with Rayleigh and Love dispersion curves and is therefore uncertain.

	Mean (m/s)	**Uncertainty (m/s)**
$V_{s,5}$	368	47
$V_{s,10}$	434	45
$V_{s,20}$	496	62
$V_{s,30}$	523	71
$V_{s,40}$	541	74
$V_{s,50}$	557	72
$V_{s,100}$	681	74
$V_{s,150}$	758	86
$V_{s,200}$	812	88

Table 7: Travel time averages at different depths from the inverted models. Uncertainty is given as one standard deviation from the selected profiles.

7.3 SH transfer function and quarter-wavelength velocity

The quarter-wavelength velocity approach [Joyner et al., 1981] provides, for a given frequency, the average velocity at a depth corresponding to 1/4 of the wavelength of interest. It is useful to identify the frequency limits of the experimental data (minimum frequency in dispersion curves at $1.25\,\mathrm{Hz}$ and in the ellipticity at $0.55\,\mathrm{Hz}$ here). The results using this proxy show that the dispersion curves constrain the profiles down to $150\,\mathrm{m}$ and the ellipticity down to $430\,\mathrm{m}$ (Fig. 13). Moreover, the quarter wavelength impedance-contrast introduced by Poggi et al. [2012a] is also displayed in the figure. It corresponds to the ratio between two quarter-wavelength average velocities, respectively from the top and the bottom part of the velocity profile, at a given frequency [Poggi et al., 2012a]. It shows a trough (inverse shows a peak) at the resonance frequency.

Moreover, the theoretical SH-wave transfer function for vertical propagation [Roesset, 1970] is computed from the inverted profiles. It is corrected with respect to the Swiss Reference Rock model [Poggi et al., 2011] following Edwards et al. [2013]. In this case, the models are predicting an amplification up to a factor of 3 at several resonance peaks. The comparison with the Empirical Spectral Modelling (ESM) amplification obtained from earthquake recordings [Edwards et al., 2013] shows a fair agreement, though only few earthquakes have been recorded yet. The ESM amplification indicates the presence of edge-generated surface waves.

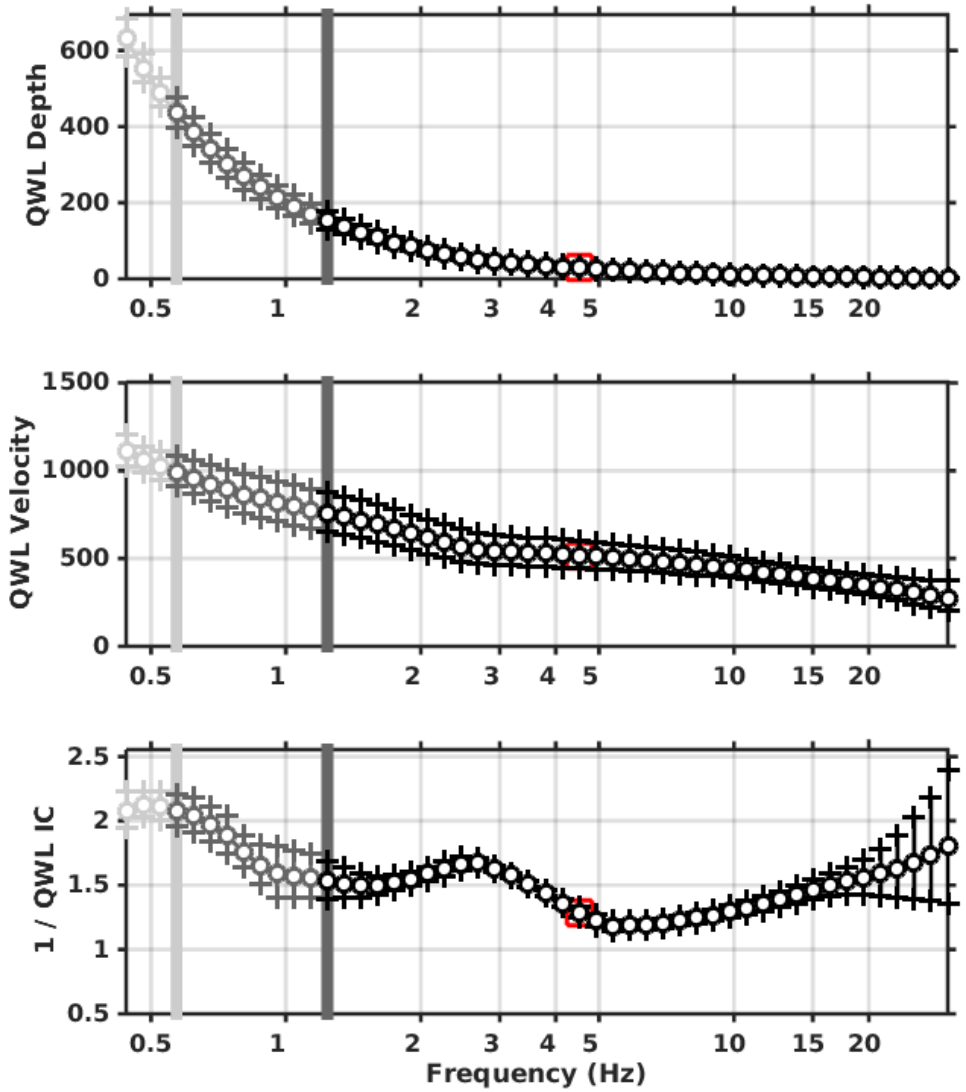

Figure 13: Quarter wavelength velocity representation of the velocity profile (top: depth, centre: velocity, bottom: inverse of the impedance contrast). Black curve is constrained by the dispersion curves, light grey is not constrained by the data. Red square is corresponding to $V_{s,30}$.

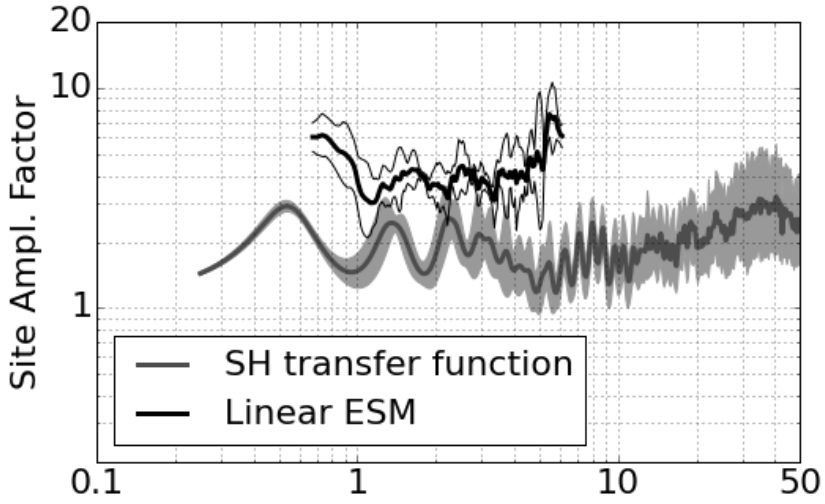

Figure 14: Theoretical SH transfer function (grey line) compared to the empirical spectral amplification [Edwards et al., 2013] (black line) with its standard deviation. Both are referenced at the Swiss Reference Rock Model [Poggi et al., 2011].

8 Conclusions

The array measurements presented in this study were successful in deriving a velocity model for the site Basel Vogelsang (SBAV station). Inversion with Love and Rayleigh dispersion curves lead to different velocity profiles. Apart from the first meter, we found a first layer of approximately $45\,\mathrm{m}$ with velocities of about $490\,\mathrm{m/s}$ using Rayleigh curves. Using Love curves, the velocity increases up to $670\,\mathrm{m/s}$ at $6\,\mathrm{m}$ depth. Profiles representative of the Rayleigh and Love dispersion curves deviate until about $200\,\mathrm{m}$ depth. Love dispersion curve provides higher velocities in this depth range, corresponding to the upper part of the Septarienton formation (Tertiary mudstone). It could be due to transverse isotropy (TIV). This kind of anisotropy is associated with layering in shales and is found where gravity is the dominant factor as it is the case for the Septarienton formation. The velocity reaches $1400\,\mathrm{m/s}$ at $400\,\mathrm{m}$ depth until the base of the Tertiary. The interface with the Mesozoic basement takes place between 550 and $650\,\mathrm{m}$ depth. It is producing the fundamental peak in the ellipticity at $0.55\,\mathrm{Hz}$.
$V_{s,30}$ is $523\,\mathrm{m/s}$, which would correspond to ground type B in the Eurocode 8 [CEN, 2004] and SIA261 [SIA, 2014] but is uncertain due to the two families of profiles used for this computation. The theoretical 1D SH transfer function computed from the inverted profiles shows amplifications up to a factor 3 at some resonance frequencies and matches the observed amplification at the station under earthquake.

Acknowledgements

The authors thank Ulrike Kleinbrod and Elias Kempf for their help during these measurements, as well as the helpline for their efficiency in towing the van.

References

Sylvette Bonnefoy-Claudet, Fabrice Cotton, and Pierre,ÄêYves Bard. The nature of noise wavefield and its applications for site effects studies. *Earth-Science Reviews*, 79(3-4): 205–227, December 2006. ISSN 00128252. doi: 10.1016/j.earscirev.2006.07.004. URL http://linkinghub.elsevier.com/retrieve/pii/S0012825206001012.

Jan Burjánek, Gabriela Gassner-Stamm, Valerio Poggi, Jeffrey R. Moore, and Donat Fäh. Ambient vibration analysis of an unstable mountain slope. *Geophysical Journal International*, 180(2):820–828, February 2010. ISSN 0956540X. doi: 10.1111/j.1365-246X.2009.04451.x. URL http://gji.oxfordjournals.org/cgi/doi/10.1111/j.1365-246X.2009.04451.xhttp://doi.wiley.com/10.1111/j.1365-246X.2009.04451.x.

J. Capon. High-Resolution Frequency-Wavenumber Spectrum Analysis. *Proceedings of the IEEE*, 57(8):1408–1418, 1969. ISSN 0018-9219. doi: 10.1109/PROC.1969.7278. URL http://ieeexplore.ieee.org/lpdocs/epic03/wrapper.htm?arnumber=1449208.

CEN. *Eurocode 8: Design of structures for earthquake resistance - Part 1: General rules, seismic actions and rules for buildings*. European Committee for Standardization, en 1998-1: edition, 2004.

Benjamin Edwards, Clotaire Michel, Valerio Poggi, and Donat Fäh. Determination of Site Amplification from Regional Seismicity : Application to the Swiss National Seismic Networks. *Seismological Research Letters*, 84(4), 2013. doi: 10.1785/0220120176.

Donat Fäh, Fortunat Kind, and Domenico Giardini. A theoretical investigation of average H/V ratios. *Geophysical Journal International*, 145(2):535–549, May 2001. ISSN 0956540X. doi: 10.1046/j.0956-540x.2001.01406.x. URL http://doi.wiley.com/10.1046/j.0956-540x.2001.01406.x.

Donat Fäh, Gabriela Stamm, and Hans-Balder Havenith. Analysis of three-component ambient vibration array measurements. *Geophysical Journal International*, 172(1):199–213, January 2008. ISSN 0956540X. doi: 10.1111/j.1365-246X.2007.03625.x. URL http://doi.wiley.com/10.1111/j.1365-246X.2007.03625.xhttp://gji.oxfordjournals.org/cgi/doi/10.1111/j.1365-246X.2007.03625.x.

Donat Fäh, Marc Wathelet, Miriam Kristekova, Hans-Balder Havenith, Brigitte Endrun, Gabriela Stamm, Valerio Poggi, Jan Burjánek, and Cécile Cornou. Using Ellipticity Information for Site Characterisation. Technical report, NERIES JRA4 Task B2, 2009.

William B. Joyner, Richard E. Warrick, and Thomas E. Fumal. The effect of Quaternary alluvium on strong ground motion in the Coyote Lake, California, earthquake of 1979. *Bulletin of the Seismological Society of America*, 71(4):1333–1349, 1981.

Katsuaki Konno and Tatsuo Ohmachi. Ground-Motion Characteristics Estimated from Spectral Ratio between Horizontal and Vertical Components of Microtremor. *Bulletin of the Seismological Society of America*, 88(1):228–241, 1998.

Stefano Maranò, C. Reller, H.-A. Loeliger, and Donat Fäh. Seismic waves estimation and wave field decomposition: Application to ambient vibrations. *Geophysical Journal International*, submitted, 2012.

Valerio Poggi and Donat Fäh. Estimating Rayleigh wave particle motion from three-component array analysis of ambient vibrations. *Geophysical Journal International*, 180(1):251–267, January 2010. ISSN 0956540X. doi: 10.1111/j.1365-246X.2009.04402.x. URL http://doi.wiley.com/10.1111/j.1365-246X.2009.04402.x.

Valerio Poggi, Benjamin Edwards, and Donat Fäh. Derivation of a Reference Shear-Wave Velocity Model from Empirical Site Amplification. *Bulletin of the Seismological Society of America*, 101(1):258–274, January 2011. ISSN 0037-1106. doi: 10.1785/0120100060. URL http://www.bssaonline.org/cgi/doi/10.1785/0120100060.

Valerio Poggi, Benjamin Edwards, and Donat Fäh. Characterizing the Vertical-to-Horizontal Ratio of Ground Motion at Soft-Sediment Sites. *Bulletin of the Seismological Society of America*, 102(6):2741–2756, December 2012a. ISSN 0037-1106. doi: 10.1785/0120120039. URL http://www.bssaonline.org/cgi/doi/10.1785/0120120039.

Valerio Poggi, Donat Fäh, Jan Burjánek, and Domenico Giardini. The use of Rayleigh-wave ellipticity for site-specific hazard assessment and microzonation: application to the city of Lucerne, Switzerland. *Geophysical Journal International*, 188(3):1154–1172, March 2012b. ISSN 0956540X. doi: 10.1111/j.1365-246X.2011.05305.x. URL http://doi.wiley.com/10.1111/j.1365-246X.2011.05305.xhttp://gji.oxfordjournals.org/cgi/doi/10.1111/j.1365-246X.2011.05305.x.

J.M. Roesset. Fundamentals of soil amplification. In R. J. Hansen, editor, *Seismic Design for Nuclear Power Plants*, pages 183–244. M.I.T. Press, Cambridge, Mass., 1970. ISBN 978-0-262-08041-5. URL http://mitpress.mit.edu/catalog/item/default.asp?ttype=2&tid=5998.

SIA. *SIA 261 Einwirkungen auf Tragwerke*. Société suisse des ingénieurs et des architectes, Zurich, Switzerland, 2014.

Marc Wathelet. An improved neighborhood algorithm: Parameter conditions and dynamic scaling. *Geophysical Research Letters*, 35(9):1–5, May 2008. ISSN 0094-8276. doi: 10.1029/2008GL033256. URL http://www.agu.org/pubs/crossref/2008/2008GL033256.shtml.